Research on infrared dim and small target detection algorithm based on low-rank tensor recovery

LIU Chuntong[1] and WANG Hao[1,2,*]

1. College of Missile Engineering, Rocket Force University of Engineering, Xi'an 710025, China;
2. Beijing Institute of Remote Sensing Equipment, Beijing 100854, China

Abstract: In order to rapidly and accurately detect infrared small and dim targets in the infrared image of complex scene collected by virtual prototyping of space-based downward-looking multiband detection, an improved detection algorithm of infrared small and dim target is proposed in this paper. Firstly, the original infrared images are changed into a new infrared patch tensor mode through data reconstruction. Then, the infrared small and dim target detection problems are converted to low-rank tensor recovery problems based on tensor nuclear norm in accordance with patch tensor characteristics, and inverse variance weighted entropy is defined for self-adaptive adjustment of sparseness. Finally, the low-rank tensor recovery problem with noise is solved by alternating the direction method to obtain the sparse target image, and the final small target is worked out by a simple partitioning algorithm. The test results in various space-based downward-looking complex scenes show that such method can restrain complex background well by virtue of rapid arithmetic speed with high detection probability and low false alarm rate. It is a kind of infrared small and dim target detection method with good performance.

Keywords: complex scene, infrared block tensor, tensor kernel norm, low-rank tensor restoration, weighted inverse entropy, alternating direction method.

1. Introduction

Space-based downward-looking multiband detection system can effectively detect and track targets and can promptly monitor and recognize the target with threat for the purpose of reliable warning [1−3]. Infrared small target detection technology in complex scenes is deemed as the core technology of space-based downward-looking detection system and a research hotspot. Infrared small target detection is difficult due to the following reasons. Firstly, small targets are often submerged in background clutter and noise, with very low signal to noise ratio (SNR) due to long viewing distance in the transmission and scattering process in the atmosphere. Secondly, small targets occupy little pixels and lack obvious texture and structure characteristics [4]. Thirdly, it is very difficult for the algorithm to balance the arithmetic speed and the detection effect [5,6]. Hence, infrared small and dim target detection is very difficult.

Currently, many infrared small target detection methods are proposed focusing on single-frame detection [7,8]. The filtering algorithm is commonly used, including the spatial high-pass filtering [9], top-hat detection based on morphology (Top-hat) [10], the largest average filtering [11], and the transform domain (frequency domain) filtering method. Those methods can reserve the edge of structured background and find targets by subtracting the predicted background after filtering from the original image, and they are applicable to the image with high signal to noise ratio and graded structure background. Such method has high false alarm rate in general. Correspondingly improved algorithms include the adaptive Top-hat filter [12], the improved bilateral filter [13], the improved Robinson Guard filter [14], and the nonnegativity-constrained variational mode decomposition [15], have improved detection performance to a certain extent. Then, another method is to start from the point of view of the target. In a single frame of infrared image, according to the target and surrounding background with the difference in features such as grayscale and structure, we can design detection operators and directly extract targets [16]. The typical method is the local contrast measurement (LCM) [17] based on the visual contrast mechanism. Since the LCM method has not been proposed for a long time, many scholars still research and improve this type of method, including multiscale patch-based contrast measure (MPCM) [18], multiscale local contrast measure (MLCM) [19], relative local contrast measure (RLCM) [20] and local difference measure (LDM) [21]. These algorithms can achieve good detection results, but

the real-time performance is poor due to pixel-by-pixel processing. Currently, the method based on data structure is widely used for small and dim target detection [22,23], in which the infrared patch-image (IPI) model [24] is the most typical one. Small targets are obtained by seeking the low-rank subspace structure and the sparsity structure of prospect data. However, such a method adopts the monad space as the background, which does not conform to the actual demands. It is not applicable for more complex background. The improved robust principal component analysis (RPCA) was proposed in [25], which divides the threshold value based on the ratio between the neighborhood sparsity mean value and the whole sparse image mean value to further eliminate the isolated noise point and the clutter of background cloud edge. The algorithm is time-consuming in the face of complex background, with high false alarm rate. A non-negative infrared patch-image model based on partial sum minimization of singular values (NIPPS) was proposed based on singular value partial sum minimization in [26]. Such method depends on the measurement of background rank in terms of accuracy, and obviously reduces performance and is time-consuming in the face of more complex background. In order to excavate more useful information from patch space, infrared patch tensor (IPT) model was proposed after expansion to tensor in [27]. Such method can greatly reduce the algorithm complexity, with high detection probability. However, the target may be lost due to larger algorithm fluctuations and low robustness. Based on the tensor nuclear norm part and non-convex approximation of rank in [28], the local feature is introduced and the infrared small and dim target detection algorithm based on tensor nuclear norm partial sum is proposed. Such a method depends on the local feature effect very well. Thus the detection effect is not very good in the face of dim target with complex background.

Hence, in order to balance the detection effect and the instantaneity better, a kind of infrared small and dim target detection method based on low-rank tensor recovery is proposed in this paper, in which the influence from noise and clutter is added to the model and the inverse variance weighted entropy as adaptive parameters is proposed to adjust sparsity. Finally, the small targets are worked out through division and positioning of threshold value. The infrared small and dim target is detected and the effectiveness of the algorithm is verified based on the test results.

2. Infrared patch tensor model

2.1 Data reconstruction of infrared image

The original gray image of infrared small target belongs to two-dimensional data, and the two-dimensional gray image shall be converted to tensor data structure. Assuming the infrared gray image is D and the tensor structure obtained after data reconstruction is $\mathcal{D}$. The data construction method shall refer to the IPI model, namely the whole image shall be browsed by sliding window. The small patch obtained each time as the obverse side slice of $\mathcal{D}$ is shown in Fig. 1.
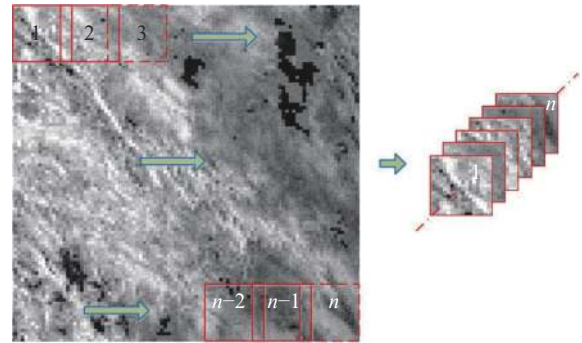

Fig. 1   Three-dimensional representation method of original infrared image

Specific reconstruction steps are as follows:

(i) The sliding window's size and step length are $m \times m$ and k, respectively. The image $D \in \mathbb{R}^{a \times b}$ is browsed from left to right and from top to bottom. The image block t with size of $m \times m$ is an obverse side slice in tensor data.

(ii) After ergodicity, assume the total sliding times of window is n. The obverse side slice obtained by image small patch constitutes the infrared patch tensor $\boldsymbol{D} \in \mathbb{R}^{m \times m \times n}$.

In practical applications, a small target usually keeps changing all the time. It is the single pixel point target and the SNR is very low in this paper. Therefore, it is small with respect to the whole image, thus the target image can be considered as a sparse matrix, which makes the corresponding target patch image still be a sparse matrix. On the other hand, due to atmospheric refraction, dispersion, optical defocusing, lens aberration, diffraction, deformation of mirror, and detector tilt, the original infrared background image tends to be slightly blurred and many local patches are approximately linearly correlated with each other even though the pixel distance between two patches may be large in an image. This property of non-local self-correlation exists commonly in infrared background images. Therefore, we can consider the background patch-image as a low-rank matrix. When the model is converted to IPT, the data changes from two-dimensional to three-dimensional, but the low rank of the background and the sparsity of the target do not change. Therefore, the background image and the target image can be obtained through tensor decomposition. Small targets can be obtained after being segmented by the threshold.

However, in IPI model, small patches in each sliding shall are converted into vectors, which breaks through the internal structure of image data so that many gray features are destroyed. Besides, such conversion mode causes large computation burden. Each small block in the window is directly used as the obverse side slice to construct data, which can guarantee the local features of image can be reserved and is conductive to withdrawing the prior information. In the meantime, the calculation efficiency of the algorithm is not influenced by the original image resolution, and is related to the size of sliding window and the sliding times. Hence, the window size and the sliding times are set reasonably in order to improve the algorithm efficiency.

The inverse process of two-dimensional image based on infrared patch tensor is opposite to the above restructuring procedures, and every obverse side slice is replaced in the original position. When the image is browsed by sliding window, the sliding step is less than the window size, and then the small block will overlap in replacement. The mean filtering method is adopted to handle with the overlapping area.

2.2 Construction of infrared patch tensor mode

In remote imaging, the point targets in infrared imagery will often be submerged in the background clutter, with low SNR to form dim targets. The target image carries very little information, causing difficulty of target detection. Such infrared image data are mainly composed of targets, the background, and noise. According to IPI model the image can be expressed as

$$f_F = f_T + f_B + f_N \tag{1}$$

where f_F, f_T, f_B, and f_N represent the input of original infrared image, target image, background image, and noise, respectively. A new IPT model can be obtained by sliding image in window

$$\mathcal{F} = \mathcal{T} + \mathcal{B} + \mathcal{N} \tag{2}$$

where $\mathcal{F}$, $\mathcal{T}$, $\mathcal{B}$, and $\mathcal{N}$ represent the IPT, target patch tensor, background patch tensor, and random noise, respectively.

In [28], three modal expansion matrices can be obtained for three-order tensor. The singular value of three expansion matrices of IPT is rapidly reduced near 0, which indicates the expansion matrix of tensor patch in each modality conforms to the low-rank nature. Hence, the background patch tensor is assumed as follows:

$$\begin{cases} \mathrm{rank}(\boldsymbol{B}_{(1)}) \leqslant r_1 \\ \mathrm{rank}(\boldsymbol{B}_{(2)}) \leqslant r_2 \\ \mathrm{rank}(\boldsymbol{B}_{(3)}) \leqslant r_3 \end{cases}$$

where $\boldsymbol{B}_{(1)}$, $\boldsymbol{B}_{(2)}$, and $\boldsymbol{B}_{(3)}$ represent the background patch tensor's model 1 expansion matrix, model 2 expansion matrix, and model 3 expansion matrix, respectively. The r_1, r_2, and r_3 are positive numbers.

They only account for a small part of pixels in infrared image in the face of dim targets. Obviously, the target patch tensor can be used as sparse tensor $\mathcal{T}$. If the noise is not considered, the background low-rank tensor and the target sparse tensor can be solved based on the following models:

$$\min_{\mathcal{B},\mathcal{T}} \ \mathrm{rank}(\mathcal{B}) + \lambda\|\mathcal{T}\|_0$$
$$\mathrm{s.t.} \ \ \mathcal{F} = \mathcal{B} + \mathcal{T} \tag{3}$$

where λ represents the regularization parameter that indicates the sparse error term weight and is used to adjust the low-rank characteristics and sparse characteristics. $\mathrm{rank}(\cdot)$ represents the matrix rank and $\|\cdot\|_0$ represents the 0 norm that indicates the number of non-zero elements in matrix. The above formula (3) is equivalent to the low-rank tensor recovery problem. Hence, infrared small and dim target detection is converted to the problems of solving the low-rank tensor recovery.

The model as mentioned above does not consider the influence from noise and clutter. As a result, the dim target detection effect will be reduced greatly in the face of infrared image in more complex scenes. In the meantime, the weighted parameters are manually set as per different scene demands, and they cannot achieve self-adaptive adjustment to avoid influencing the detection effect. Hence, a kind of more robust tensor recovery method is proposed in this paper, and a reweighted strategy is added to recover the low-rank and sparse tensor of existing noise and clutter. The improved model can be expressed as

$$\min_{\mathcal{B},\mathcal{T},\mathcal{N}} \ \mathrm{rank}(\mathcal{B}) + \lambda_a\|\mathcal{T} \odot \mathcal{W}_s\|_0 + \gamma\|\mathcal{N}\|_F^2$$
$$\mathrm{s.t.} \ \ \mathcal{F} = \mathcal{B} + \mathcal{T} + \mathcal{N} \tag{4}$$

where λ_a, γ, and $\mathcal{W}_s$ indicate the self-adaptive weighted parameters, the weight of random noise, the reweighted patch tensor respectively. The $\|\cdot\|_F^2$ indicates F normal which is used to depict the random noise.

3. Infrared small and dim target detection based on recovery of low-rank tensor

3.1 Priori model

Traditional infrared dim and small target detection methods focus on the design of filters and most of them only focus on the extraction of local features, such as local

contrast [29], local entropy and local difference [30], which cannot distinguish the background from the target. The structure tensor is used to construct the priori information W_1 and W_2 of local structure in [27] and [28]. However, such detection effect will be limited to the local

prior results. Hence, for the dim targets with lower SNR, the result based on local prior information will leak detection targets, causing the poor final detection effect. Two kinds of local prior information conditions based on image SNR of 3 are shown in Fig. 2.
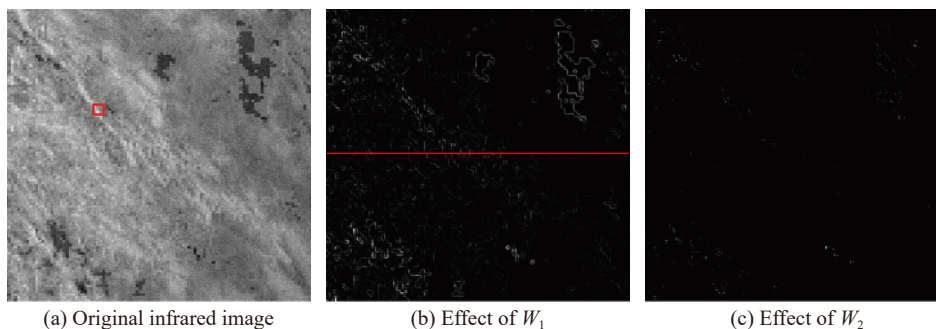

(a) Original infrared image   (b) Effect of W_1 (c) Effect of W_2

Fig. 2   Local priori effect

Fig. 2 shows that faced with the infrared dim and small target image with an SNR of 3, the targets are all missed after the prior effect of local features. In the meantime, many background edges exist in the prior role of W_1, which will cause the increase of algorithm operating time. Hence, the prior restrictions of this part are taken out in this paper. However, in order to accelerate the rate of convergence of model and reduce the target detection time, the reweighted strategy is selected and a sparse weight $\mathcal{W}_s$ is added

$$\mathcal{W}_s^{k+1} = \frac{1}{|\mathcal{T}^k| + \upsilon} \tag{5}$$

where υ is a small positive number used to prevent denominator as 0, and k indicates the iterations times.

3.2   Inverse variance weighted entropy

Infrared small and dim target image background in different scenes is complex. Different gray values change in different background areas, in which the gray in dim target field scope changes acutely in general, while the gray in background field scope changes gently. Hence, the selection of fixed weighted parameters will inevitably influence the detection effect based on the gray change in different scenes. The inverse variance weighted entropy H is introduced as the self-adaptive weighted parameter, namely the weighted parameter λ_a is set adaptively based on the image complexity change of different scenes to adjust the sparsity and achieve the dim target detection better. The expression formula of H is

$$H = -\sum_{i=0}^{L-1}\{q(z_i - \bar{z}) \cdot p(z_i) \cdot \log_2(1 - p(z_i) + \upsilon)\} \tag{6}$$

where q, z_i, $\bar{z}$, and $p(z_i)$ represent the weighted factor, the ith gray value, the overall gray mean value and the

occurrence probability of gray value z_i in image. υ is a very positive number to ensure that $\log_2(1 - p(z_i) + \upsilon)$ still exists in the case of $p(z_i) = 1$.

Literature [31] points out that the inverse entropy function meets the non-negativity, symmetry and extremum property. When z_i meets the even distribution, the inverse entropy function can obtain the minimal value. In other words, when the image gray value changes fiercely and the gray scope is wide, the inverse entropy is small and the image complexity is large; while when the image changes flatly and the gray value is very collective, the inverse entropy is large and the image complexity is small. Inverse entropy is inversely proportional to the image complexity and is directly proportional to the cost function sparse weight λ. Hence, based on the $\lambda_a = H$ as self-adaptive weighted parameters and their relationship, the contact between image complexity and target detection algorithm is preliminarily discussed.

3.3   Algorithm solution

The low-rank property of background patch tensor is described based on the sum of nuclear norms (SNN) by reference of the single case model in reweighted infrared patch-tensor (RIPT). In order to solve the model, norm 1 replaces norm 0 for relaxation processing. Hence, the convex optimization model is finally solved as follows:

$$\min_{\mathcal{B},\mathcal{T},\mathcal{N}} \sum_{i=1}^{3}\left\|\mathcal{B}_{(i)}\right\|_* + \lambda_a\|\mathcal{T} \odot \mathcal{W}_s\|_1 + \gamma\|\mathcal{N}\|_F^2$$

$$\text{s.t.} \quad \mathcal{F} = \mathcal{B} + \mathcal{T} + \mathcal{N}. \tag{7}$$

The alternating direction method of multipliers (ADMM) is selected to solve the separable convex optimization problem. It can improve the rate of convergence and accuracy due to the dim condition conver-

gence of multiplier method and the separable decomposability of dual ascent. In order to solve the model, the Lagrange function in (7) can be constructed

$$\mathcal{L} = \sum_{i=1}^{3} \|\mathcal{B}_i\|_* + \lambda_a \|\mathcal{T} \odot \mathcal{W}_s\|_1 + \gamma \|\mathcal{N}\|_F^2 +$$
$$\sum_{i=1}^{3} \frac{1}{2\mu} \|\mathcal{B}_i + \mathcal{T} + \mathcal{N} - \mathcal{F}\|_F^2 - \langle \mathcal{Y}_i, \mathcal{B}_i + \mathcal{T} + \mathcal{N} - \mathcal{F} \rangle \quad (8)$$

where $\mathcal{Y}$, μ, and $\langle \cdot \rangle$ represent the Lagrange multiplier, penalty factor and inner product among tensors.

Based on ADMM, $\mathcal{L}$ can be broken into several sub-problems for iterative update.

(i) Fixation of the rest of the variables and update of $\mathcal{B}_i$.

$$\mathcal{B}_i^{k+1} = \arg\min_{\mathcal{B}_i} \|\mathcal{B}_i\|_* +$$
$$\frac{\mu^k}{2} \left\| \mathcal{B}_i - \left(\mathcal{F} - \mathcal{T}^k - \mathcal{N}^k + \mu^{-k} \mathcal{Y}^k \right) \right\|_F^2 \quad (9)$$

(ii) Fixation of the rest of the variables and update of $\mathcal{T}$.

$$\mathcal{T}^{k+1} = \arg\min_{\mathcal{T}} \lambda_a \|\mathcal{T} \odot \mathcal{W}_s\|_1 +$$
$$\sum_{i=1}^{3} \frac{\mu^k}{2} \left\| \mathcal{T} - \left(\mathcal{F} - \mathcal{B}_i^{k+1} - \mathcal{N}^{k+1} + \mu^{-k} \mathcal{Y}^k \right) \right\|_F^2 \quad (10)$$

(iii) Fixation of the rest of the variables and update of $\mathcal{N}$.

$$\mathcal{N}^{k+1} = \arg\min_{\mathcal{N}} \gamma \|\mathcal{N}\|_F^2 +$$
$$\sum_{i=1}^{3} \frac{\mu^k}{2} \left\| \mathcal{F} - \mathcal{B}_i^{k+1} - \mathcal{T}^{k+1} + \mu^{-k} \mathcal{Y}^k \right\|_F^2 \quad (11)$$

(iv) Fixation of the rest of the variables and update of $\mathcal{Y}_i^{k+1}$.

$$\mathcal{Y}_i^{k+1} = \mathcal{Y}_i^k + \frac{1}{\mu^k} \left(\mathcal{F} - \mathcal{B}_i^{k+1} - \mathcal{T}^{k+1} - \mathcal{N}^{k+1} \right), \quad i = 1, 2, 3 \quad (12)$$

(v) Update of parameters: $\mu^{k+1} = \mu^k / \rho$.

(vi) Inspection of termination condition.

$$\frac{\left\| \mathcal{F} - \mathcal{B}^{k+1} - \mathcal{T}^{k+1} - \mathcal{N}^{k+1} \right\|_F}{\|\mathcal{F}\|_F} < \varepsilon \ \text{ or } \ \left\| \mathcal{T}^{k+1} \right\|_0 = \left\| \mathcal{T}^k \right\|_0 . \quad (13)$$

4. Experimental results and analysis

The data adopted in this paper are from the simulation of space-based downward-looking detection system, namely the high sky-to-ground complex background and the border background. The simulation is based on a real detection scene to establish a working environment, via the mathematical model to simulate the photoelectric imaging process (effect) for algorithm evaluation. All target and scene data are modeled and simulated mainly through the energy conversion of detection system virtual prototype, not actual satellite images. However, the simulated data has been compared and evaluated with the actual satellite data by Beijing Institute of Remote Sensing Equipment. The complexity, spatial noise and other indicators are not less than 90% authenticity. It has a high degree of realism. It can be used as real data. Fig. 3 shows the infrared image of four kinds of different scenes, including three kinds of ground scenes and one kind of border scene, in which the border scene gives three frames of images, including the target in three different situations. The detailed information is shown in Table 1. All images are 14 bits.
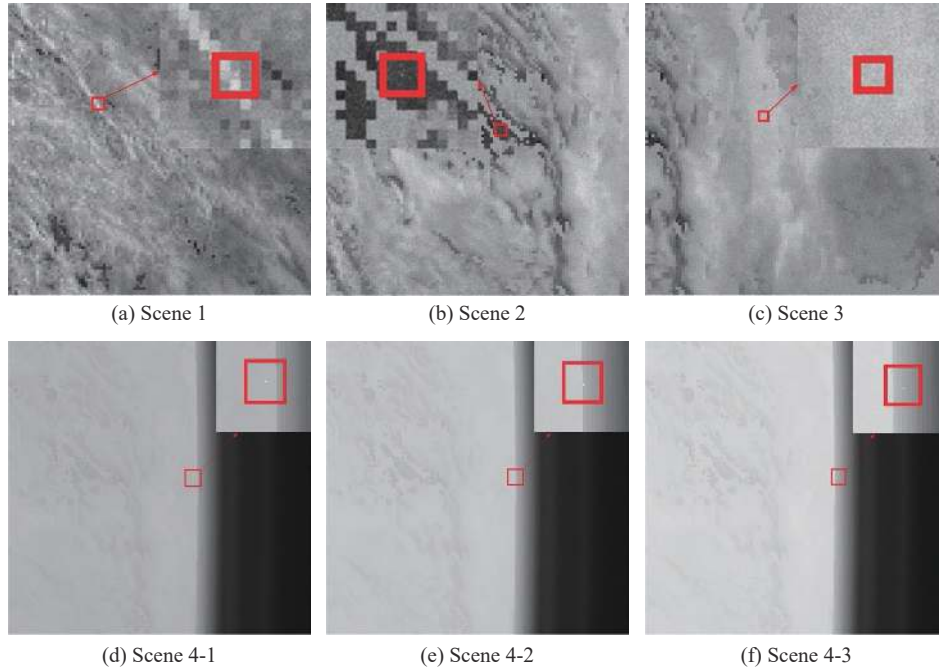

| (a) Scene 1 | (b) Scene 2 | (c) Scene 3 |

| (d) Scene 4-1 | (e) Scene 4-2 | (f) Scene 4-3 |

Fig. 3   Examples of the experimental sequence images

Table 1   Details of each scene

Image	Sensor	Resolution	SNR	Detail
Sequence 1	Infrared	640×640	3	Single pixel point target is in the hilly area
Sequence 2	Infrared	640×640	3	Single pixel point target is in the water lake area
Sequence 3	Infrared	640×640	3	Single pixel point target is in the cloud area
Sequence 4	Infrared	640×640	1	Single pixel point target is around the border

All four scenes are infrared images and the target is tail flame information, single pixel. The ground scene 1 aims at the hilly area around which the gray value fluctuates greatly and changes fiercely; the ground scene 2 aims at the lake area whose adjacent scope has certain contrast ratio, but around which there is edge background, relatively complex; the ground scene 3 aims at the cloud area which belongs to the highlighted area; the border scene involves the highlighted stable background, border change background and high contrast background of object in three different kinds of circumstances from left to right, so that the algorithm can guarantee the target can be effectively detected in three kinds of scenes around limb when detection system tests the tracking target, and the target can keep stable without disappearing in the detection and tracking process.

In the test, the Matlab R2019a, Inter Core i7-8550U and 8 GB memory are adopted as text platform. The signal to clutter ratio gain (SCRG), background suppression factor (B_f), time consuming (t), true positive rate (TPR) and false alarm rate (FAR) are selected as the evaluation index of the algorithm. SCRG, B_f, TPR and FAR are defined as follows:

$$SCRG = \frac{SCR_{out}}{SCR_{in}} \qquad (14)$$

$$B_f = \frac{(\sigma_\beta)_{in}}{(\sigma_\beta)_{out}} \qquad (15)$$

$$\begin{cases} TPR = \dfrac{\text{true positive samples}}{\text{positive sample set}} \\ FAR = \dfrac{\text{false positive samples}}{\text{sample set}} \end{cases} \qquad (16)$$

where SCR_{out}, SCR_{in}, $(\sigma_\beta)_{in}$, and $(\sigma_\beta)_{out}$ represent the signal to clutter ratio of output part, the signal to clutter ratio of input data, the background gray value standard deviation of original image and the background response value standard deviation of response diagram, respectively.

Firstly, by reference of infrared image of small and dim target in the hilly area, different regularization parameters are valued and detection results are researched, as shown in Fig. 4. The research results show that the background clutter cannot be restrained well, with many false alarms if the parameters are small. The target cannot be detected if the parameters are large. Hence, it is very important to adaptively adjust parameters in different scenes, which avoids the manual setting, and avoids poor detection results due to setting deviation.
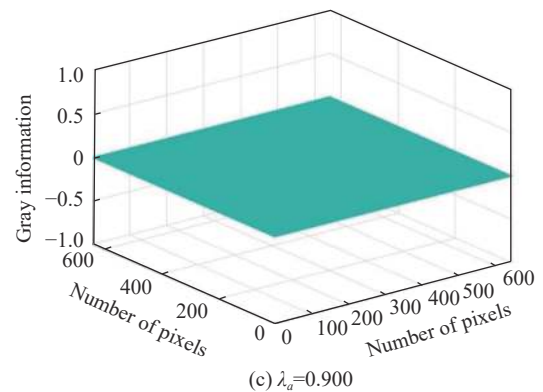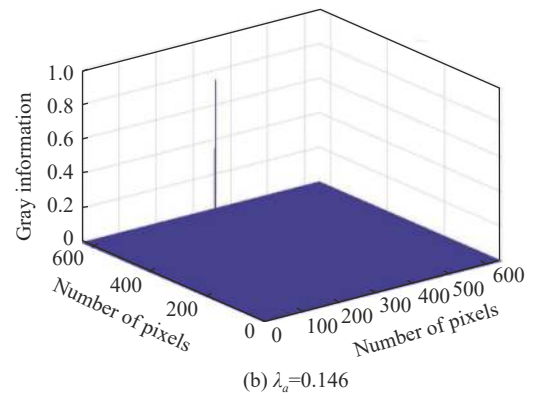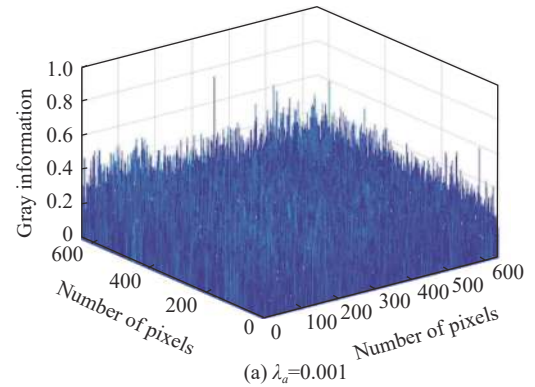
Fig. 4   Three-dimensional gray-scale response map of detection results for different regularization parameters

Later, in order to verify the superiority of the method in infrared small target detection, the proposed algorithm in this paper is compared with the Top-hat algorithm [10], LCM algorithm [17], NIPPS algorithm [24], RIPT algorithm [25], and PSTNN algorithm [26], with the algorithm background suppression results shown in Fig. 5– Fig. 10 (the image sequence corresponds to Fig. 3).

(a) Scene 1   (b) Scene 2   (c) Scene 3

(d) Scene 4-1   (e) Scene 4-2   (f) Scene 4-3
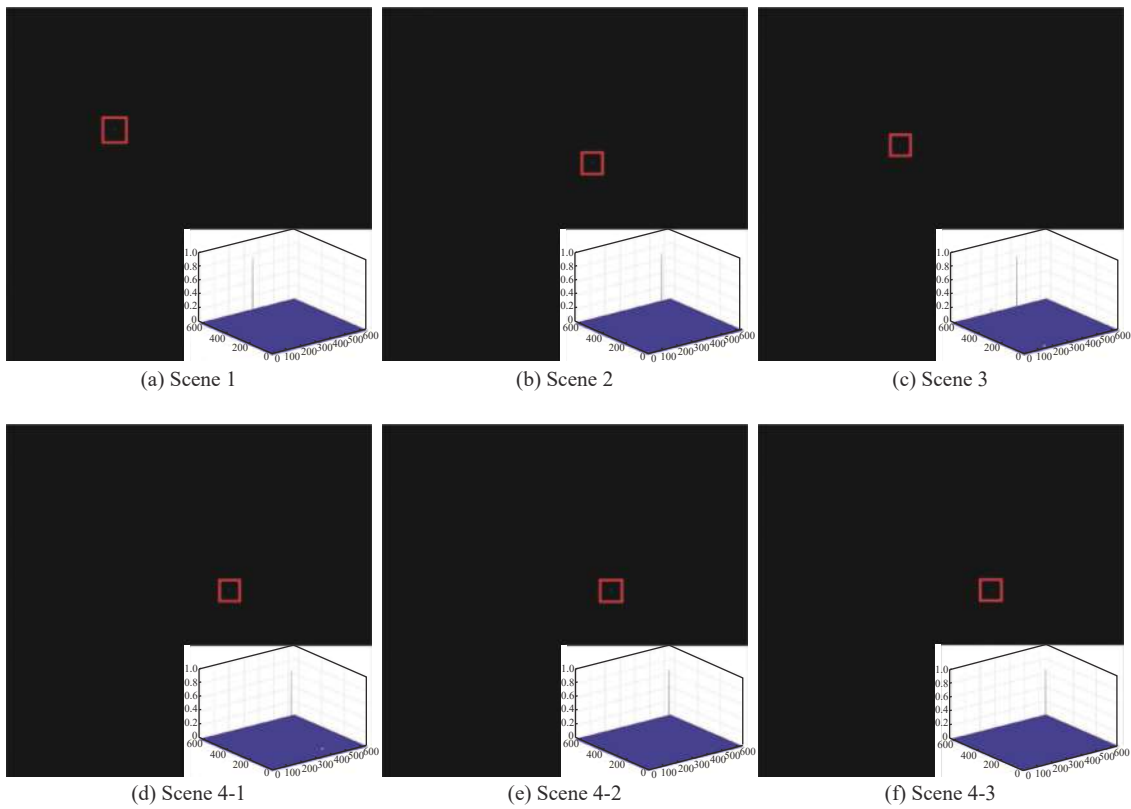
Fig. 5   Results of the proposed algorithm

(a) Scene 1   (b) Scene 2   (c) Scene 3

(d) Scene 4-1   (e) Scene 4-2   (f) Scene 4-3
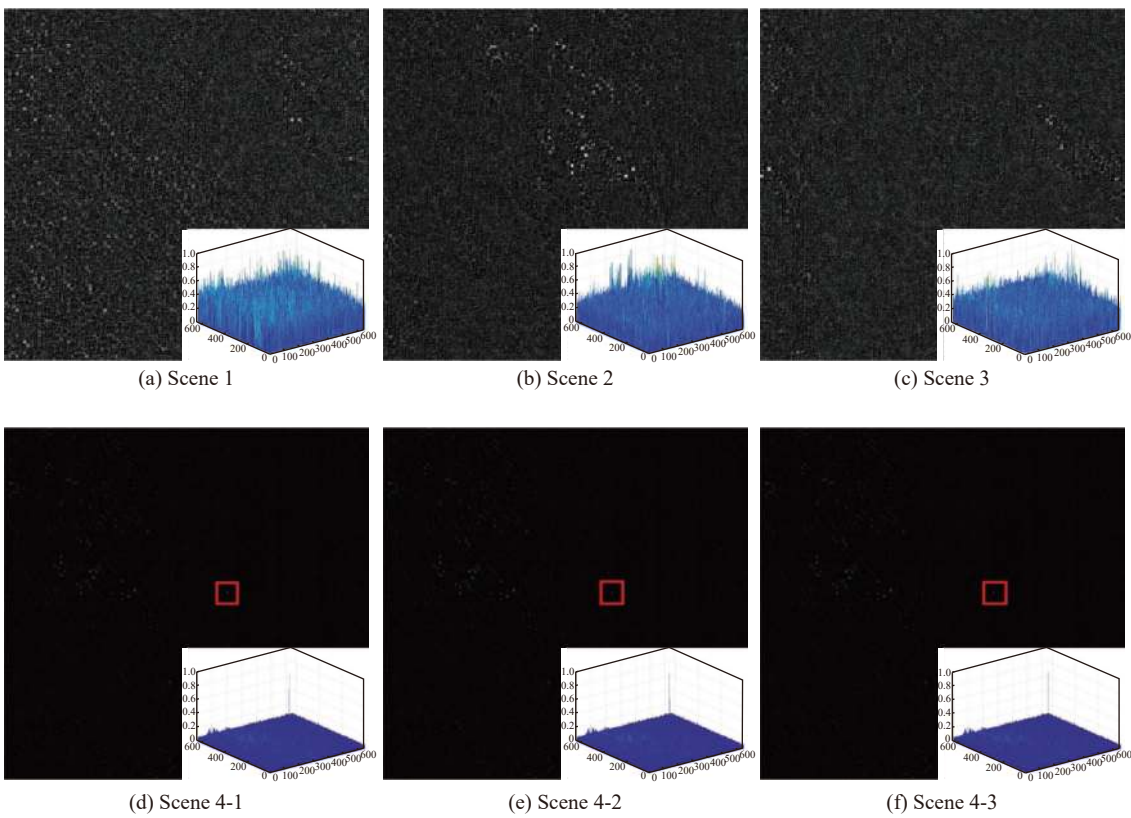
Fig. 6   Results of the Top-hat algorithm

(a) Scene 1   (b) Scene 2   (c) Scene 3

(d) Scene 4-1   (e) Scene 4-2   (f) Scene 4-3
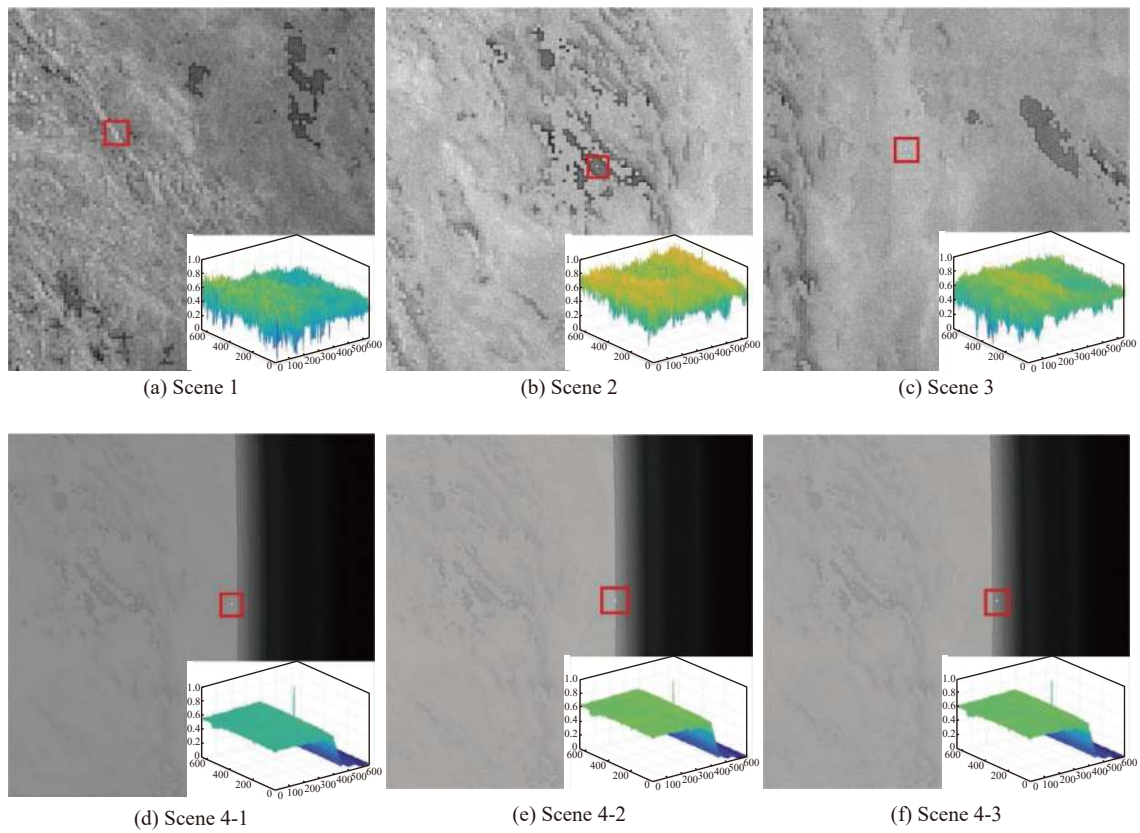
Fig. 7   Results of the LCM algorithm

(a) Scene 1   (b) Scene 2   (c) Scene 3

(d) Scene 4-1   (e) Scene 4-2   (f) Scene 4-3
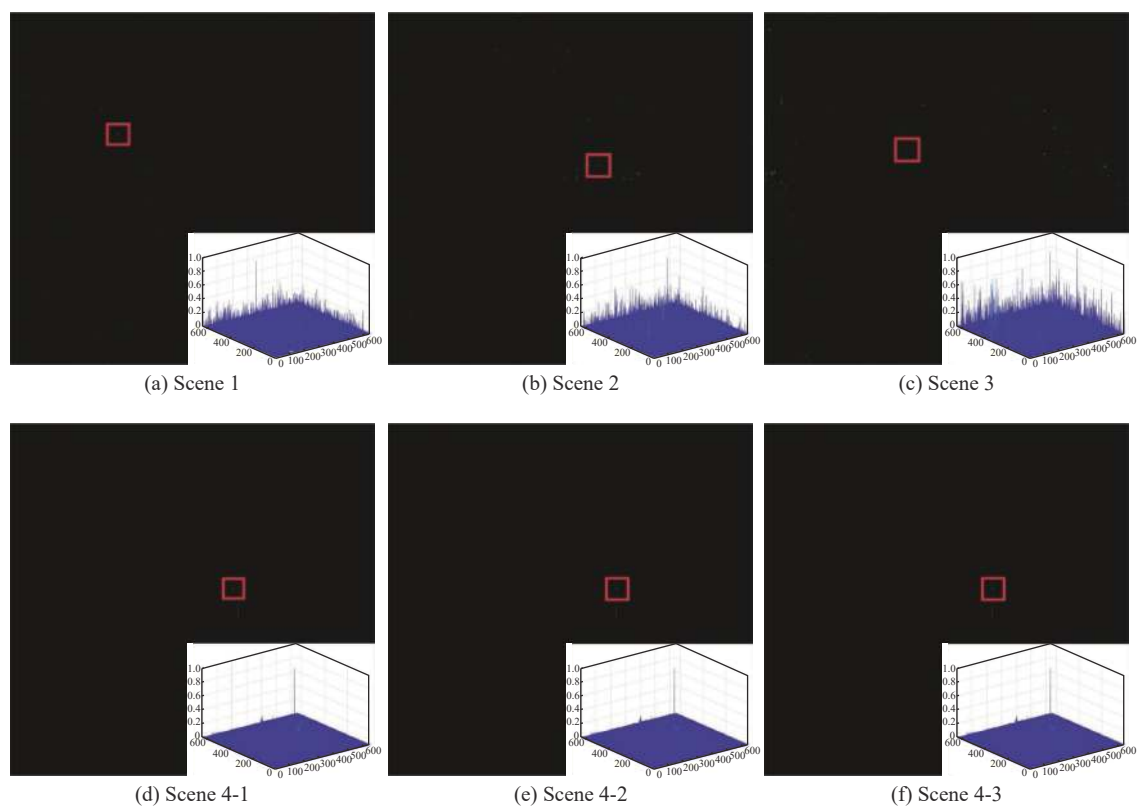
Fig. 8   Results of the NIPPS algorithm

(a) Scene 1   (b) Scene 2   (c) Scene 3

(d) Scene 4-1   (e) Scene 4-2   (f) Scene 4-3
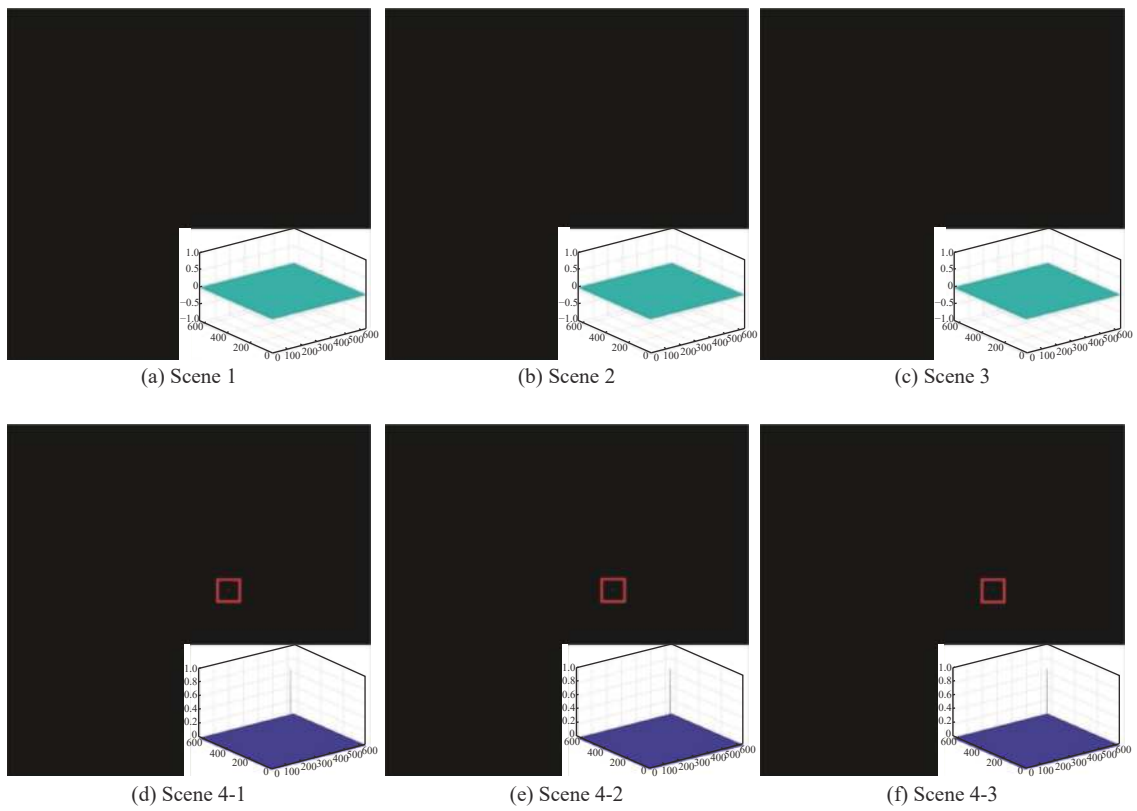
Fig. 9   Results of the RIPT algorithm

(a) Scene 1   (b) Scene 2   (c) Scene 3

(d) Scene 4-1   (e) Scene 4-2   (f) Scene 4-3

Fig. 10   Results of the PSTNN algorithm

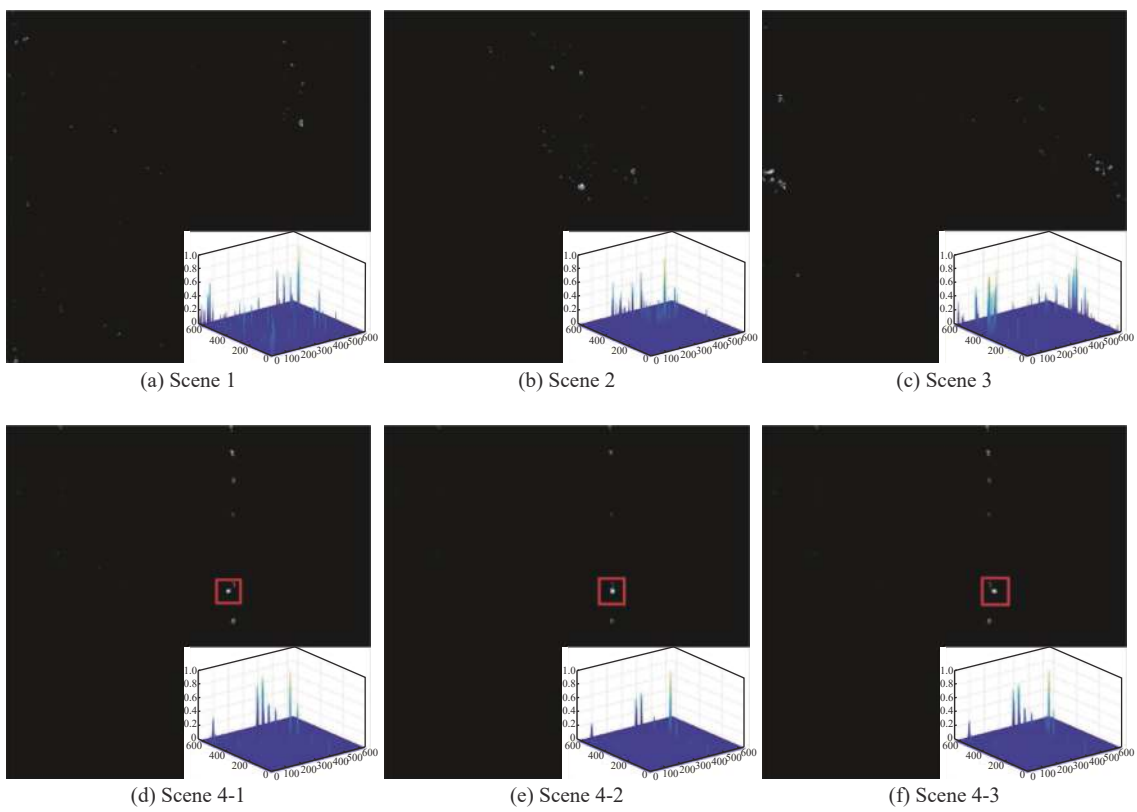Fig. 5−Fig. 10 show that for the small and dim target in ground and border complex scene, the algorithm in this paper can restrain background and noise very well and highlights the target; the background suppression effect of the Top-hat algorithm includes two kinds of conditions, in which the ground scene has poor effect with many background clutter and the object is not enhanced obviously, while the limb scene has good background suppression and the object is enhanced very well. There is only a small part of background residue; the LCM algorithm utilizes the local contrast mechanism to relatively obviously enhance target, but the general background suppression effect will cause many false alarms; the NIPPS algorithm plays a certain role in background suppression in the ground scene, with target enhanced, but many clutters in scene easily bring many false alarms. While the limb scene effect is good; both RIPT and PSTNN algorithms utilize the local transcendental characteristics for low-rank tensor recovery. Restricted by local feature, small and dim targets in ground scene are all missed. Although the limb scene has the certain background suppression effect, the target size increases in the limb scene background suppression of PSTNN. The effect needs to be improved.

On the other hand, in order to evaluate the algorithm performance more objectively, Table 2, Table 3, and Table 4 list the index comparison of the SCRG, background suppression factor (B_f) and time consuming (t) for different algorithms, in which NaN indicates the numerical result makes mistakes and the Inf indicates the data value is great. It is observed that there is the maximum SNR gain and the minimum background suppression factor in this method. Hence, the corresponding suppression effect is the best and the subsequent detection results will be more accurate. In the meantime, with regard to the operating time, although the scene consumes a little longer time than Top-hat, the background suppression effect is better and the false alarm is less, which can balance the detection effect and operation time better.

Table 2   SCRG comparison of different algorithms

Method	Scene					
	Scene 1	Scene 2	Scene 3	Scene 4-1	Scene 4-2	Scene 4-3
Top-hat	1.09	1.02	2.07	3.79	19.03	40.66
LCM	4.82	5.67	10.87	24.58	10.44	23.78
NIPPS	70.44	259.67	123.34	29.50	25.19	117.56
RIPT	NaN	NaN	NaN	534.31	418.24	746.13
PSTNN	3.10	1.05	2.65	2.66	8.27	14.83
Proposed	438.93	639.53	497.69	Inf	Inf	Inf

Table 3 B_f comparison of different algorithms

Method	Scene					
	Scene 1	Scene 2	Scene 3	Scene 4-1	Scene 4-2	Scene 4-3
Top-hat	0.92	0.83	0.99	0.07	0.06	0.05
LCM	0.76	0.80	0.73	0.78	0.83	0.76
NIPPS	0.10	0.09	0.16	0	0.01	0.01
RIPT	NaN	NaN	NaN	0	0	0
PSTNN	0.13	0.12	0.19	0.04	0.03	0.03
Proposed	0	0	0	0	0	0

Table 4 t comparison of different algorithms   s

Method	Scene					
	Scene 1	Scene 2	Scene 3	Scene 4-1	Scene 4-2	Scene 4-3
Top-hat	0.89	0.88	0.87	0.98	0.98	0.91
LCM	12.72	9.14	8.86	8.86	8.62	8.77
NIPPS	618.71	619.26	613.05	612.90	614.34	611.72
RIPT	5.61	7.01	5.89	4.43	4.09	4.18
PSTNN	59.79	59.95	60.29	71.36	71.36	69.98
Proposed	3.90	3.83	3.71	3.78	3.81	4.09

The regularization parameter value of the algorithm in different scenes, as shown in Table 5, also reflects the weighted inverse entropy in different scenes and shows that the value of ground scene is less than that of limb scene and the ground scene is obviously complex than the limb scene, with greater detection difficulty. The complexity of different background changes in ground scene is slightly different and the small and dim targets have the most complex image in small lake. However, the border scene shows the existing problems, namely the same image target has different detection results at different positions, but their complexity is the same. Hence, with regard to the design of complexity, more aspects can be improved and researched in the future.

Table 5   Regularization parameter values in different scenarios

Parameter	Value
λ_1	0.15
λ_2	0.11
λ_3	0.12
λ_{4-1}	0.36
λ_{4-2}	0.36
λ_{4-3}	0.36

Finally, for the sequence image in six kinds of scenes, each kind of sequence contains 30 frames. The total number of image frames reaches 180 and the number of actual targets reaches 180. The self-adaptive threshold value is adopted in each kind of method to divide

response diagram and to count the quantity of detection targets and false alarm targets as well as to calculate the detection rate TPR and false alarm rate FAR, as shown in Table 6. The result shows that RIPT and PSTNN cause lower target detection probability due to local prior restriction. The NIPPS' detection effect is relatively good. The algorithm proposed has the optimal detection performance, with higher detection rate and lower false alarm rate.

Table 6 TPR and FAR of different algorithms

Rate	Method					
	Top-hat	LCM	NIPPS	RIPT	PSTNN	Proposed
TPR	0.512	0.685	0.691	0.524	0.429	0.947
FAR	0.401	0.418	0.432	0.509	0.614	0.053

5. Conclusions

A kind of infrared small target detection algorithm based on the low-rank tensor recovery is proposed in this paper for the actual application background of space-based downward-looking detection system in the ground and border complex scene. Reconstruct the original infrared image data, complete the construction of a low-rank tensor model, add a reweighted strategy, define adaptive regularization parameters, and solve the model to complete target detection. The test results show that the method can be applicable to the single-pixel small and dim target infrared image of complex scenes for the simulated data. It can be a potential detection algorithm. According to the actual data in the future, the method can be further optimized.

References

[1] JIANG T X, HUANG T Z, ZHAO X L, et al. Multi-dimensional imaging data recovery via minimizing the partial sum of tubal nuclear norm. Journal of Computational and Applied Mathematics, 2020, 372: 112680.

[2] ZHANG W C, CHEN J, GAO Y. Infrared small and dim target detection based on weighted nuclear norm minimization. Ordnance Industry Automation, 2018, 37(6): 7. (in Chinese)

[3] FAN Z L, BI D Y, XIONG L, et al. Dim infrared image enhancement based on convolutional neural network. Neurocomputing, 2018, 272: 396−404.

[4] LIU M Q, HUANG Z C, FAN Z, et al. Infrared dim target detection and tracking based on particle filte. Proc. of the 36th Chinese Control Conference, 2017: 5372−5378.

[5] BAI X Z, BI Y G. Derivative entropy-based contrast measure for infrared small-target detection. IEEE Trans. on Geoscience and Remote Sensing, 2018, 56(4): 2452−2466.

[6] WANG W X, FU Y T, DONG F, et al. Infrared ship target detection method based on deep convolution neural network. Acta Optica Sinica, 2018, 38(7): 0712006.

[7] MARVASTI F S, MOSAVI M R, NASIRI M. Flying small target detection in IR images based on adaptive toggle operator. IET Computer Vision, 2018, 12(4): 527−534.

[8] WANG X Y, PENG Z M, ZHANG P, et al. Infrared small

target detection via nonnegativity-constrained variational mode decomposition. IEEE Gecscience and Remote Sensing Letters, 2017, 14(10): 1700−1704.

[9] PENTLAND A P. Fractal-based description of natural scenes. IEEE Trans. on Pattern Analysis and Machine Intelligence, 1984, 6(6): 661−674.

[10] TOM V T, PELI T, LEUNG M, et al. Morphology-based algorithm for point target detection in infrared backgrounds. Proc. of the Optical Engineering and Photonics in Aero-space Sensing, 1993: 2−11.

[11] DESHPANDE S D, MENG H E, VENKATESWARLU R, et al. Max-mean and max-median filters for detection of small targets. Proc. of the SPIE's International Symposium on Optical Science, Engineering, and Instrumentation, 1999: 74−83.

[12] DENG L Z, ZHU H, ZHOU Q, et al. Adaptive top-hat filter based on quantum genetic algorithm for infrared small target detection. Multimedia Tools and Applications, 2018, 77(9): 10539−10551.

[13] ZHANG Y, TIAN X, REN P. An adaptive bilateral filter based framework for image denoising. Neurocomputing, 2014, 140(22): 299−316.

[14] ZHANG S F, HUANG X H, WANG M. Background suppression algorithm for infrared images based on robinson guard filter. Proc. of the 2nd International Conference on Multimedia and Image processing, 2017: 250−254.

[15] WANG X Y, PENG Z M. ZHANG P, et al. Infrared small target detection via nonnegativity-constrained variational mode decomposition. IEEE Geoscience and Remote Sensing Letters, 2017, 14(10): 1700−1704.

[16] YI X, WANG B J, ZHOU H X, et al. Dim and small infrared target fast detection guided by visual saliency. Infrared Physics & Technology, 2019, 97: 6−14.

[17] CHEN C L P, LI H, WEI Y T, et al. A local contrast method for small infrared target detection. IEEE Geoscience Remote Sensing Letters, 2014, 52(1): 574−581.

[18] WEI Y T, YOU X G, LI H. Multiscale patch-based contrast measure for small infrared target detection. Pattern Recognition, 2016, 58: 216−226.

[19] NIE J Y, QU S C, WEI Y T, et al. An infrared small target detection method based on multiscale local homogeneity measure. Infrared Physics & Technology, 2018, 90: 186−194.

[20] HAN J H, LIANG K, ZHOU B, et al. Infrared small target detection utilizing the multiscale relative local contrast measure. IEEE Geoscience and Remote Sensing Letters, 2018, 15(4): 612−616.

[21] DENG H, SUN X P, LIU M L, et al. Small infrared target detection based on weighted local difference measure. IEEE Trans. on Geoscience and Remote Sensing, 2016, 54(7): 4204−4214.

[22] QIAN K, ZHOU H X, WANG B J, et al. Infrared dim moving target tracking via sparsity-based discriminative classifier and convolutional network. Infrared Physics & Technology, 2017, 86: 103−115.

[23] SUN Y, YANG J G, LONG Y L, et al. Infrared small target detection via spatial-temporal total variation regularization and weighted tensor nuclear norm. IEEE Access, 2019, 7: 56667−56682.

[24] GAO C Q, MENG D Y, YANG Y, et al. Infrared patch-image model for small target detection in a single image. IEEE Trans. on Image Processing, 2013, 22(12): 4996−5009.

[25] MA M Y, WANG D J, SUN H, et al. Infrared dim-small target detection based on robust principal component analysis and multi-point constant false alarm. Acta Optica Sinica, 2019, 39(8): 0810001.

[26] DAI Y M, WU Y Q, SONG Y, et al. Non-negative infrared

patch-image model: robust target-background separation via partial sum minimization of singular values. Infrared Physics & Technology, 2017, 81: 182–194.

[27] DAI Y M, WU Y Q. Reweighted infrared patch-tensor model with both nonlocal and local priors for single-frame small target detection. IEEE Journal of Selected Topics in Applied Earth Observations and Remote Sensing, 2017, 10(8): 3752–3767.

[28] ZHANG L D, PENG Z M. Infrared small target detection based on partial sum of the tensor nuclear norm. Remote Sensing, 2019, 11(4): 382.

[29] DU P, HAMDULLA A. Infrared small target detection using homogeneity-weighted local contrast measure. IEEE Geoscience and Remote Sensing Letters, 2019, 17(3): 514–518.

[30] GAO J Y, GUO Y L, LIN Z P, et al. Robust infrared sm all target detection using multiscale gray and variance difference measures. IEEE Journal of Selected Topics in Applied Earth Observations and Remote Sensing, 2018, 11(12): 5039–5052.

[31] KANG H, XIA M. Detectability of infrared small targets. Infrared Physics & Technology, 2010, 53: 208–217.

Biographies

LIU Chuntong was born in 1972. He received his B.S., M.S., and Ph.D degrees in the Rocket Force University of Engineering, Xi'an, China, in 1993, 1996 and 2009, respectively. He is currently with the Rocket Force University of Engineering, China. His major research interests include photoelectric technology and optical fiber sensing technology and application.
E-mail: liuchuntong72@sina.com

WANG Hao was born in 1991. He received his B.S and M.S degrees in the Rocket Force University of Engineering, Xi'an, China, in 2014 and 2017, respectively. He is currently with the Rocket Force University of Engineering, China. His major research interests include infrared small and dim target detection technology.
E-mail: 17791821514@163.com